

# CFD analysis of melting and evaporation of Tin in different EBVG cavities

Anik Mazumder, Sanjay Sethi\*

Beam Technology Development Group,  
Bhabha Atomic Research Centre, Mumbai-400 085, India

## Abstract

Electron beam vapour generators (EBVG) are widely used for melting and evaporation applications of metals. Due to the high operating temperature and vacuum boundaries, often the experimental characterization of melting and evaporation of metals in EBVG cavities becomes challenging. Computational analysis provides important insights of such physical phenomena. In this study, the melting and evaporation of tin was studied in three different EBVG cavities. These cavities can accommodate a total charge volume of 30cc, 70cc and 110cc. An in-house general purpose CFD solver AnuPravaha was used for CFD simulation of melting and evaporation phenomena. The peak temperature under the e-beam, molten pool profile and evaporation rate of tin was compared for the three systems. The effect of solid metal oxide at the molten pool surface on the molten pool profile and evaporation rate was also studied. It was observed that there was marginal decrease of evaporation rate as the cavity volume was increased due to the change in convection current. The molten pool fraction increased in 70cc and 110cc cavities due to the change in aspect ratio. It was also observed that due to the presence of solid oxide on the surface, the molten fraction and the evaporation rate of tin increased marginally. The molten pool profile also changed due to the solid oxide layer. This phenomena can be attributed to the change of convection current profile at the molten metal surface.

**Keywords:** E-beam, Electron beam vapour generator, CFD, melting, metal evaporation

## Introduction

Electron beam vapour generators (EBVG) have been extensively used for applications like physical vapour deposition (PVD), laser based isotopic purification processes (LIS) etc. [1-3]. Specially for melting and evaporation applications of high melting point and low vapour pressure metals, electron guns are often considered as the most suitable energy source owing to their high energy intensities [4-5]. Therefore, understanding the phase change phenomena of metals in the EBVG cavity has great significance for optimization of the aforementioned processes. Due to the high temperature of the system, it is often difficult to resolve the phenomena experimentally. Hence, researchers have often taken recourse to the numerical solutions along with experiments for better understanding of the system.

Melting and evaporation of different metals in electron beam gun systems has

been studied extensively in literature. Westerberg and McClelland [6] has studied the effect of heat conduction and natural convection for an electron beam cold-hearth re-melting system both experimentally and with modified Galerkin finite-element method. Westerberg et al. [7] studied the evaporation of Ti and Ti-6Al-4V both experimentally and computationally and found the evaporation rate and their linear variation with e-beam power. They also observed that the computationally calculated evaporation rates were much higher than the experimentally observed value. Owing to the current focus in additive manufacturing, selective electron beam melting (SEBM) has been studied numerically using the lattice-Boltzmann method (LBM) [8, 9].

In this study, the melting and evaporation of tin have been analysed computationally with in-house developed general purpose CFD solver AnuPravaha. AnuPravaha is a finite volume solver

developed in C++ platform with the capability of addressing problems from various domains of fluid flow and heat transfer [10-12]. The software has the capability of solving CFD problems over the hybrid unstructured mesh to accommodate for complex geometry without any coordinate transformation [13]. The development and experimental validation of the phase change module of AnuPravaha solver has been reported by our group elsewhere [14].

In this paper, the melting and evaporation of tin in three different EBVG cavities of volume 30cc, 70cc and 110cc was studied. For laser based isotopic purification processes, the molten fraction inside the cavity is a significant process parameter [15]. Maximization of molten pool ensures the maximum participation of charge atoms in the metal vapour and increases the efficiency of isotopic purification. Hence, as an important process parameter, the molten pool fraction of tin for the three cavities were compared to access the effect of geometry on molten fraction. We also compare the maximum temperature under the electron beam and evaporation rate of tin for the three systems. Due to the high operating temperature of the system, most metallic systems in EBVG cavity consists of a surface layer of metallic oxide. During the e-beam evaporation, the oxide layer remains solid due to its high melting point. The effect of the presence of this solid oxide layer on the evaporation rate was also estimated computationally in this study.

## Physical phenomena in an EBVG cavity

A general schematic of a 270° bend EBVG is shown in Figure 1. In such an EBVG system, the charge material to be evaporated is contained in a liner crucible which is placed in a water cooled copper cavity. The total system is kept inside a vacuum chamber where a chamber pressure of  $\sim 1 \times 10^{-5}$  mbar is maintained

Energy balance equation

For the enthalpy-porosity technique, the energy balance equation is formulated for the total enthalpy of the system. For 2-D axis-symmetric geometry, the equation is as follows

$$\rho \left( \frac{\partial h}{\partial t} + u_z \frac{\partial h}{\partial z} + u_r \frac{\partial h}{\partial r} \right) = \frac{1}{r C_p} \frac{\partial}{\partial r} \left( r k \frac{\partial h}{\partial r} \right) + \frac{1}{C_p} \frac{\partial}{\partial z} \left( k \frac{\partial h}{\partial z} \right) \quad (1)$$

In the enthalpy porosity technique, the total enthalpy gets divided into sensible enthalpy ( $h_s$ ) and latent enthalpy ( $h_l$ ). While sensible enthalpy is used as a variable in the energy equation, the latent enthalpy is considered as a source term. It gets updated depending on the liquid fraction ( $f$ ) of each cell after each time step. Simplifying equation (1) in terms of the two enthalpies finally boils down to the following

$$\frac{\partial}{\partial t} (\rho h_s) + \frac{\partial}{\partial z} (\rho u_z h_s) + \frac{\partial}{\partial r} (\rho u_r h_s) = \frac{k}{C_p} \left( \frac{\partial^2 h_s}{\partial z^2} + \frac{\partial^2 h_s}{\partial r^2} \right) + \frac{k}{C_p} \left( \frac{\partial h_s}{\partial r} \right) - \frac{\rho u_r h_s}{r} - \rho \left( \frac{\partial h_l}{\partial t} \right) \quad (2)$$

Where the last three terms on the right hand side can be considered as source term, while the rest of the equation can be solved as 2-D energy equation.

In the source term, the latent enthalpy ( $h_l$ ) is described as a function of temperature. In the case of isothermal phase change,

$$h_l = f(T) = L ; \text{ when } T > T_m$$

$$\text{and } h_l = 0 ; \text{ when } T < T_m$$

where,  $T_m$  is the melting point of the solid, and  $L$  is the latent heat of enthalpy. In the enthalpy-porosity technique, the solid-liquid interface need not be tracked separately as it emerges as a part of the solution itself.

The momentum equations:

The two momentum equations for radial and axial velocity are as follows

$$\rho \left( \frac{\partial u_r}{\partial t} + u_r \frac{\partial u_r}{\partial r} + u_z \frac{\partial u_r}{\partial z} \right) = - \frac{\partial p}{\partial r} + \mu \left[ \frac{1}{r} \frac{\partial}{\partial r} \left( \frac{\partial u_r}{\partial r} \right) + \frac{\partial^2 u_r}{\partial z^2} - \frac{u_r}{r^2} \right] + S_r - A u_r \quad (3)$$

$$\rho \left( \frac{\partial u_z}{\partial t} + u_r \frac{\partial u_z}{\partial r} + u_z \frac{\partial u_z}{\partial z} \right) = - \frac{\partial p}{\partial z} + \mu \left[ \frac{1}{r} \frac{\partial}{\partial r} \left( \frac{\partial u_z}{\partial r} \right) + \frac{\partial^2 u_z}{\partial z^2} \right] + S_z - A u_z \quad (4)$$

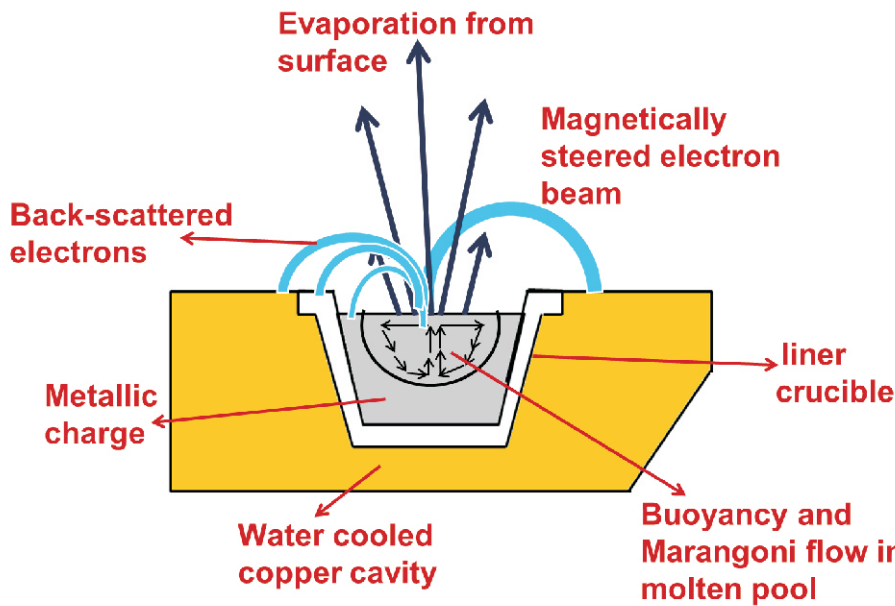


Fig. 1: Schematic of physical phenomena in EBVG cavity.

during EB operations. The electrons are generated by thermionic emission of a filament generally made of refractory metal. By virtue of an applied electric field, the electrons accelerate and form an electron beam which is then magnetically steered to the charge surface after providing a 270° bend. As the e-beam interacts with the charge metal, some fraction of the electron beam gets reflected from the surface which is referred as “back-scattered” electrons. These electrons undergo elastic collisions with the atoms of the charge. The rest of the electrons undergo inelastic collision with the charge atoms and their kinetic energy is deposited to the charge as heat. As the temperature of the surface reaches the melting temperature of the charge, the charge starts melting. As the molten pool volume increases, we observe the buoyancy driven natural convection flow in the bulk liquid. Due to the thermal gradient of surface tension, Marangoni flow can be observed at the liquid surface. Depending on the vapour pressure of the charge, evaporation of metal starts from the surface of the liquid pool when the temperature is sufficiently high. As the metal vapour leaves the liquid surface, it gives a back-thrust on the liquid surface. If the intensity of the back-thrust is significant, it can deform the liquid surface and may lead to a key-hole formation. But for applications like e-beam melting or vapour generator, the intensity of back-thrust is kept nominal and the liquid surface may be assumed to be flat.

Simulation of evaporation of tin in EBVG

The e-beam evaporation of tin inside an EBVG cavity was modelled in AnuPravaha with the following assumptions:

1. The heat flux from the electron beam was modelled as a surface heat flux with Gaussian intensity.
2. Density variation in the liquid pool was incorporated through Boussinesq approximation as the density variations in liquid metals are within the range of ±5% [16].
3. The electron beam spot was considered to be stationary.
4. Evaporation was modelled as a heat sink i.e. mass loss due to evaporation was not accounted. This assumption is valid for a quasi-steady state which is applicable where the evaporated mass is negligible compared to the total mass of the system.
5. The liquid surface was assumed to be flat and back-thrust was neglected.
6. The flow of liquid metal was assumed to be laminar.

Modelling of phase change phenomena

For modelling of the phase change phenomena for melting in the e-beam cavity, enthalpy-porosity technique [17] was used in AnuPravaha. The modelling of 2-D axis-symmetric solver for laminar flow has been described here, and a very similar approach was taken for 2-D and 3-D solvers.

Where,  $S_r$  and  $S_z$  contain any additional source term like buoyancy in radial and axial direction, respectively. The term  $A$  is defined as

$$A = \frac{C(1-f)^2}{f^3} \quad (5)$$

Where “ $C$ ” is the morphology constant with a large value and “ $f$ ” is the liquid fraction of the cell. This term is used to differentiate between the solid and liquid phase. In the solid domain, due to its large value, the velocity is forced to zero. On the other hand, in the liquid domain, this term itself attains zero value.

The continuity equation and the other boundary conditions were implemented in a conventional way into the solver. We will discuss the implementation of concentrated beam boundary condition in details.

### Surface heat flux boundary condition for electron beam

There are four different phenomena under the electron beam

1. Absorption of electron beam: after the back-scattered and transmitted particles go unused, a fraction of the total beam power is absorbed at the surface. The absorbed power was assumed to have a Gaussian profile.
2. Convection heat loss from the surface.
3. Radiation loss from the surface.
4. Evaporation loss from the surface: If the latent heat of evaporation is  $\gamma$ , the evaporation heat loss per unit area will be  $Q_{evap} = \dot{m} \lambda$ . Where  $\dot{m}$  is the evaporative mass loss per unit area per unit time.

The evaporative mass loss can be calculated from the vapour pressure and velocity data, which will be a strong function of temperature.

Combining the four phenomena mentioned above together, we can construct an energy balance equation as follows:

$$k \frac{\partial T}{\partial n} = P_{abs} - \sigma \varepsilon (T_b^4 - T_{amb}^4) - h(T_b - T_{amb}) - \lambda \dot{m} \quad (6)$$

$T_b$  is the boundary temperature.

$T_{amb}$  is the ambient temperature

$h$  is the heat transfer coefficient for convective losses along with the other conventional symbols.

We can observe that equation 6 can be written with only  $T_b$  as the unknown variable and can be solved using an appropriate root-finding algorithm. In AnuPravaha solver, Ridder's method [18] was used as the root-finding algorithm for finding the value of  $T_b$  and thereafter, the value can be used like a Dirichlet boundary.

With the aforementioned modelling approach of axis-symmetric flow and surface heat flux, the domain was discretized using the finite volume method. A pseudo-transient approach was implemented in the solver for solving both steady and unsteady problems over hybrid unstructured grid.

### EBVG cavities with different volumes dimensions and boundary conditions

In this study, 3 different EBVG cavities were considered for computational analysis. The total volume of charge that can be accommodated inside these cavities are 30cc, 70cc and 110cc respectively. During the evaporation of tin, graphite crucible was used to contain the charge. A typical schematic of charge metal inside the liner crucible is shown in Fig. 2.

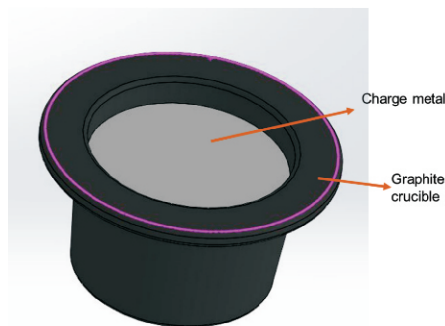


Fig. 2: Charge metal contained in a graphite crucible.

The 2D axi-symmetric view of the three EBVG systems consisting of charge and liner crucible has been shown in Fig. 3 along with the dimensions.

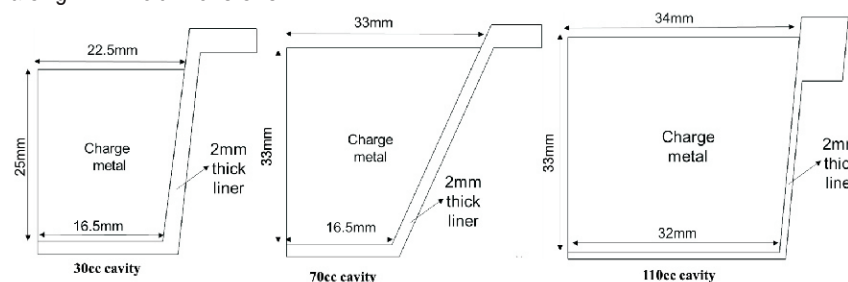


Fig. 3: 2D axi-symmetric geometry for the three EBVG cavities with dimensions.

The boundary conditions used for the numerical solution of fluid flow and heat transfer is shown in Fig. 4 for the respective boundaries.

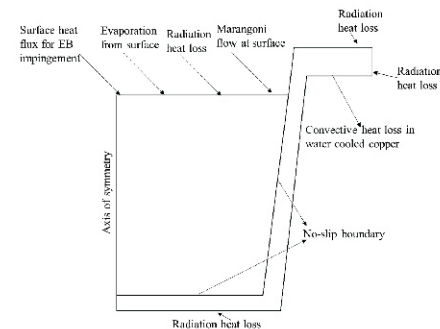


Fig. 4: The boundary conditions with the respective boundaries.

The e-beam evaporation of tin has been numerically solved for all these 3 geometries for e-beam power ranging from 1000W-1800W. The powers were selected based on the typical evaporation rates used for related applications. The temperature under the e-beam, evaporation rate of tin and molten fraction of the total charge was compared for the three systems.

### Modelling the solid oxide layer on the surface of molten pool

Due to the high operating temperature of the system, the charge metal gets oxidized after repeated evaporation cycle even inside vacuum chamber. Due to their relatively high melting points, the metal oxides remain in solid phase under electron beam. As a result, two distinct zone appear at the surface of the charge. Metallic zone at the center and oxide layer at the periphery as shown in Fig. 5.

In a CFD problem, the solid oxide layer can be modelled as a “no-slip” boundary condition at the periphery. Due to this no slip boundary condition, the convection current at the surface is also likely to be changed which is likely to affect the system parameters like evaporation rate. The model is also shown in Fig. 5 in an axi-

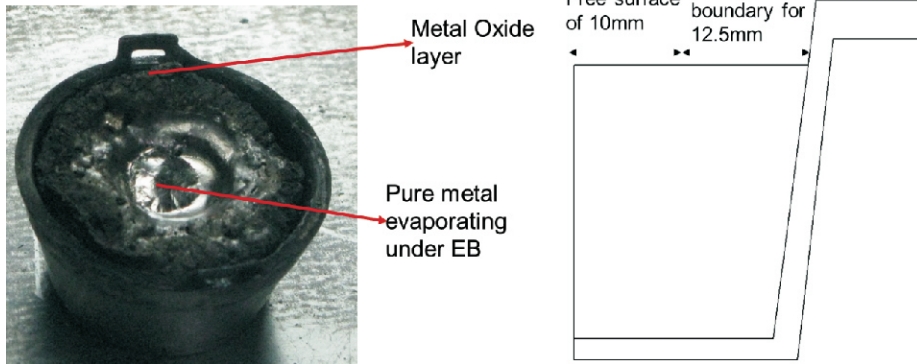


**Fig. 5:** An image of metallic oxide layer at the surface for tin and modelling of oxide layer as “no-slip” boundary.

symmetric domain. In this study, the molten pool profile with and without the oxide layer is compared for evaporation of tin in a 30cc cavity with 1000W EB power. The evaporation rates for both the systems were also compared.

**Results and Discussions**

*Molten fraction of the total charge*

The fraction of the total charge melted under the steady-state condition under each e-beam power was recorded. The variation of molten pool fraction for 70cc and 110cc cavity is shown in Figure 6 and Figure 7 respectively.

It was observed that the molten pool fraction does not change significantly with increasing EB power for the system under consideration in the operating range of power. The computationally obtained

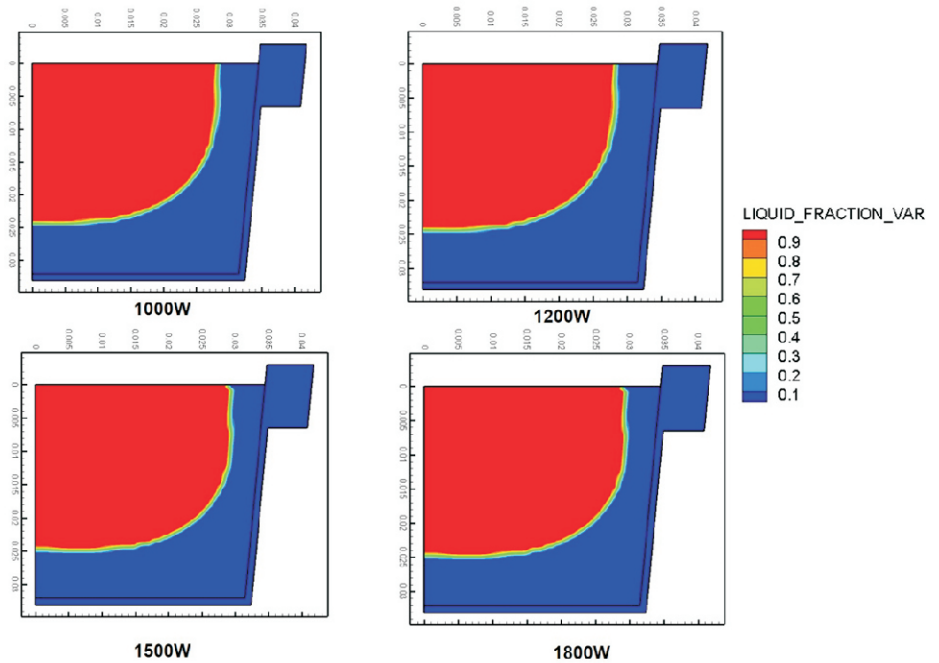


**Fig. 7:** Variation of molten pool fraction in 110cc cavity for 4 different EB power.

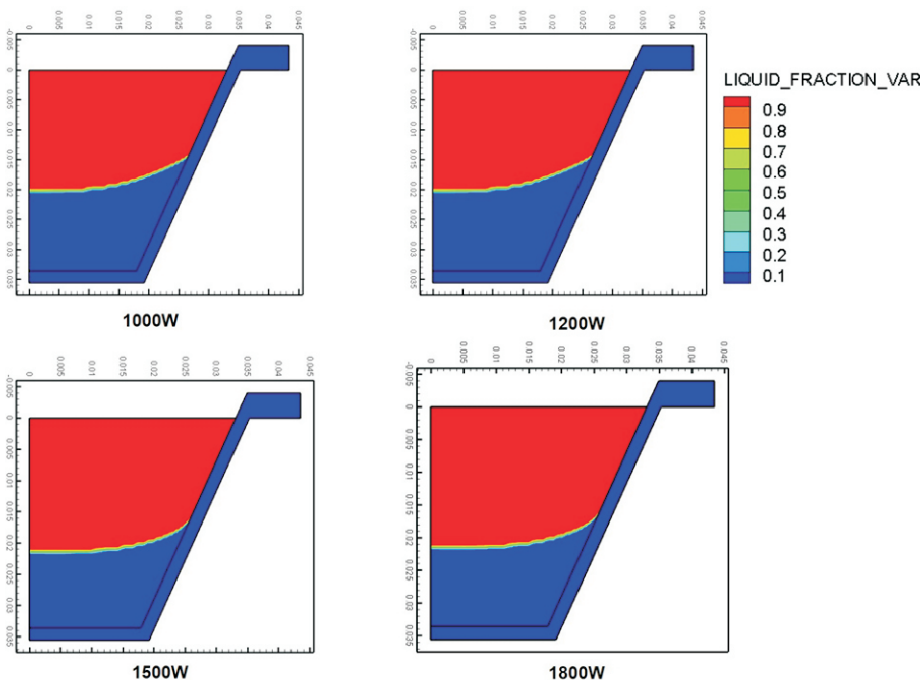


**Fig. 6:** Variation of molten pool fraction in 70cc cavity for 4 different EB power.

maximum temperature under the e-beam and the evaporation rate of tin for the three different system at different e-beam power is listed in Table 1.

From the results in Table 1, we can observe that the peak temperature and the evaporation rate reduces marginally as we increase the size of the cavity. Due to the increase of the cavity size, the distance between the heat source and heat sink changes. The change of the convection current due to this geometrical change can be identified as the reason behind the changed thermal profile. However, we can

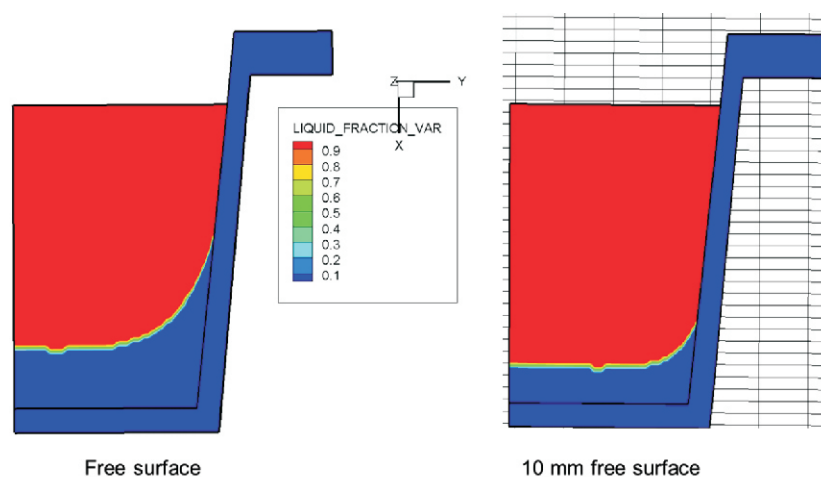
see that the molten fraction increases as we go from 30cc to 70cc and 110cc systems. Although marginal, this increase is probably due to the aspect ratio of the charge. From Fig. 6 and 7, we can identify that melting the bottom portion of the charge becomes challenging at all e-beam power. As the 30cc system has larger depth than radius, the molten fraction is relatively low. On the contrary, in 70cc and 110cc systems, the depth is nearly equal to the radius, which increases the molten fraction of the system. This phenomena can also be attributed to the change in convection current profile which assists in heat transfer to the bottom portion of the geometry in larger EBVG cavities.

*Effect of oxide layer on molten pool profile and evaporation rate.*

For evaporation of tin with e-beam power of 1000W, the molten pool profile

**Table 1: Variation of temperature, evaporation rate and molten fraction with e-beam power at different EBVG cavities.**

	Power (W)	Evaporation rate (g/h)	Maximum temperature (°C)	Molten fraction
30cc	1000	110	2345	45%
	1200	215	2468	47%
	1500	460	2610	47%
	1800	780	2700	48%
70cc	1000	100	2340	54%
	1200	212	2463	55%
	1500	450	2600	55%
	1800	750	2690	55%
110cc	1000	80	2320	56%
	1200	200	2450	57%
	1500	420	2590	58%
	1800	700	2670	58%

**Fig. 8: Molten pool profile with free surface (no oxide layer) and 10mm free surface at center (Oxide layer in periphery).****Table 2: Comparison of computationally obtained process parameters with and without the oxide layer at surface.**

Parameter	Without oxide layer	With oxide layer
Molten pool fraction	45%	49%
Peak Temperature (°C)	2345	2365
Evaporation rate (g/h)	110	130

with and without the “no-slip” oxide layer was compared. The molten pool profiles are shown in Figure 8.

The comparison of molten pool fraction, peak temperature and evaporation rates with and without the oxide layer is shown in Table 2.

From Figure 8, we can observe that the bottom profile of the molten pool changes from a parabolic shape to a flat shape in presence of solid oxide layer. From Table 2, we can also observe that the peak temperature and evaporation rate also increases in presence of oxide layer. The

phenomena can be attributed to the fact that the convection current at the surface breaks down due to the solid oxide layer. Hence, the convective heat transfer to the periphery reduces. This increases the peak temperature and also increases the heat transfer to the bottom part nominally. As a result, we can observe an increase in both the molten fraction and the evaporation rate.

### Conclusions

Melting and evaporation of tin in EBVG cavity was studied with an in-house general purpose CFD solver AnuPravaha. Three

different EBVG cavities with different volumes were considered for analysis to estimate the effect of cavity geometry. It was observed that the evaporation rate and peak temperature under the beam reduces marginally when the cavity size increases. The change in the convection current profile was identified as the probable reason. It was also observed that, the molten pool fraction increases when the radius of the cavity is equal to or greater than the depth. Here also, the change in the convection current profile assists in the heat transfer to the bottom portion of the geometry for larger cavities. The effect of solid metal oxide layer on the melting and evaporation was also accessed with a “no-slip” boundary condition. It was observed that the molten pool profile changes due to the presence of metal oxide at the surface. The evaporation rate and molten fraction also increases marginally when the solid oxide is present in the system. This phenomena was attributed to the breakage of convection current due to solid oxide layer at the molten pool surface.

### Acknowledgements

Authors acknowledge with thanks the support provided by Associate Director, Beam Technology Development Group, BARC. The authors are also thankful to Venkat P.P.K, Computer Division, BARC for providing immense support with AnuPravaha. The authors express their sincere gratitude to Prof. Amaresh Dalal, Prof Ganesh Natarajan (Mechanical Engg, IITG), Prof Arnab Atta (Chemical Engg, IIT KGP), and Nagaraj Alangi, BARC for their inputs and guidance towards this work.

### Corresponding Author\*

Sanjay Sethi (s\_sethi@barc.gov.in)

### References

- [1] Rahmani, H. and Cabanas, I.L., 2019. Development of alloy coatings by electron beam physical vapour deposition method. *Surface Engineering*, pp.1-9.
- [2] Ali, N., Teixeira, J.A., Addali, A., Saeed, M., Al-Zubi, F., Sedaghat, A. and Bahzad, H., 2019. Deposition of Stainless Steel Thin Films: An Electron Beam Physical Vapour Deposition Approach. *Materials*, **12(4)**, p.571.
- [3] Bokhan, P.A., Buchanov, V.V., Fateev, N.V., Kalugin, M.M., Kazaryan, M.A.,

- Prokhorov, A.M. and Zakrevskii, D.E., 2006. *Laser isotope separation in atomic vapor*. John Wiley & Sons.
- [4] Asano, T., Uetake, N. and Suzuki, K., 1992. Mean atomic velocities of uranium, titanium and copper during electron beam evaporation. *Journal of Nuclear Science and Technology*, **29(12)**, pp.1194-1200.
- [5] Schiller, S., Heisig, U. and Panzer, S., 1982. *Electron beam technology*. John Wiley & Sons.
- [6] Westerberg KW, McClelland MA. Modeling of material and energy flow in an EBCHR casting system. Lawrence Livermore National Lab., CA (United States); 1994 Nov 1.
- [7] Westerberg, K.W., Merier, T.C., McClelland, M.A., Braun, D.G., Berzins, L.V., Anklam, T.M. and Storer, J., 1998. Analysis of the e-beam evaporation of titanium and Ti-6Al-4V (No. UCRL-JC-128692; CONF-9710176-). Lawrence Livermore National Lab., CA (United States).
- [8] Helmer, H., Bauereiß, A., Singer, R.F. and Körner, C., 2016. Grain structure evolution in Inconel 718 during selective electron beam melting. *Materials Science and Engineering: A*, **668**, pp.180-187.
- [9] Klassen, A., Forster, V.E., Juechter, V. and Körner, C., 2017. Numerical simulation of multi-component evaporation during selective electron beam melting of TiAl. *Journal of Materials Processing Technology*, **247**, pp.280-288.
- [10] Manik, J., Parmanand, M., Kotoky, S., Borgohain, P., Dalal, A. and Natarajan, G., 2017. Lessons from anupravaha: Towards a general purpose computational framework on hybrid unstructured meshes for multi-physics applications. In Proceedings of CHT-17 ICHMT International Symposium on Advances in Computational Heat Transfer. Begel House Inc..
- [11] Manik, J., Dalal, A. and Natarajan, G., 2018. A generic algorithm for three-dimensional multiphase flows on unstructured meshes. *International Journal of Multiphase Flow*, **106**, pp.228-242.
- [12] Parmananda, M., Dalal, A. and Natarajan, G., 2018. The influence of partitions on predicting heat transfer due to the combined effects of convection and thermal radiation in cubical enclosures. *International Journal of Heat and Mass Transfer*, **121**, pp.1179-1200.
- [13] Dalal, A., Eswaran, V. and Biswas, G., 2008. A finite-volume method for Navier-Stokes equations on unstructured meshes. *Numerical Heat Transfer, Part B: Fundamentals*, **54(3)**, pp.238-259.
- [14] Mazumder, A., Garg, T., Dalal, A. and Sethi, S., Development of a phase change solver for concentrated energy beam applications. (Submitted to *International communications for heat and mass transfer* in June, 2021)
- [15] Mukherjee, J., Sethi, S., Anupama, P., Dey, S.P., Nagaraj, A., Das, D.R., Kumar, D., Verma, M.K., Karmakar, K., Barnwal, T.A. and Yadav, S.P., 2015. Study of condensation and flow of liquid metal for laser based purification processes. In Proceedings of the international thorium energy conference: gateway to thorium energy.
- [16] Brandes, Eric A., and G. B. Brook, eds. *Smithells metals reference book*. Elsevier, 2013.
- [17] Brent, A.D., Voller, V.R. and Reid, K.T.J., 1988. Enthalpy-porosity technique for modeling convection-diffusion phase change: application to the melting of a pure metal. *Numerical Heat Transfer, Part A Applications*, **13(3)**, pp.297-318.
- [18] McGuire, T., 1994. Equation solving by Ridders' method. *Stata Technical Bulletin*, **3(17)**.